Vacuum 164 (2019) 381–389

Contents lists available at ScienceDirect

Vacuum

journal homepage: www.elsevier.com/locate/vacuum

Movement of luminous group spots on target and size modification of micro-particles during cathodic vacuum arc deposition

Xiao Zuo[a,1], Rende Chen[a,1], Dong Zhang[a], Peiling Ke[a,b], Aiying Wang[a,b,*]

[a] Key Laboratory of Marine Materials and Related Technologies, Zhejiang Key Laboratory of Marine Materials and Protective Technologies, Ningbo Institute of Materials Technology and Engineering, Chinese Academy of Sciences, Ningbo, 315201, China

[b] The Center of Materials Science and Optoelectronics Engineering, University of Chinese Academy of Sciences, Beijing, 100049, China

A B S T R A C T

Modification of micro-particle size during cathodic arc deposition is an important issue for the preparation of hard coatings and nanomaterials. In this work, a coil winding and permanent magnets were applied to adjust the magnetic field of a cathodic arc source. The motion of luminous group spots was investigated through high speed imaging method. The average size of the spots was reduced with the decrease of arc current. When the arc current was higher than 80 A, the size probability distributions of the spots presented as bimodal functions. But it turned into unimodal functions at lower arc currents. By changing the coil current three kinds of spots position distributions were observed, such as centered distribution, intermediate and periphery annulus distributions. Their corresponding spots movements were stochastic, spiral and circular motion dominated. The influence of magnetic field on the spots motion was discussed. Although the average spots size was reduced with the increase of coil current to 2.5 A. Further increasing the coil current leaded to a gathering of spots towards the periphery region of the cathode surface, and an increase of the spots size. Finally, a relationship between the spots size and micro-particles size was established.

1. Introduction

Metal-vapor cathodic vacuum arcs (MCVAs) have the ability to produce high density metallic plasma. High ionization fraction of metal vapors provides sufficient energetic ions for coating deposition [1]. Therefore, the application of cathodic vacuum arc deposition has been received many attentions in the preparation of nanocomposite materials [2,3], and hard coatings [4,5] like TiAlSiN, TiN, and TiB_2 coatings, etc. However, this method suffers a main drawback during deposition processes, which is the emission of micro-droplets [6,7]. The resultant micro-particles in the deposited coatings have significant impacts on surface morphology, microstructure, and physical properties [8,9]. Meanwhile, when go beyond as harmful species for hard coatings, the micro-particles can be very useful for the preparation of nanomaterials. MCVAs deposition method has been used to produce self-organized metal nanoparticles with significant consequences for catalytic properties [10]. S.H. Kim et al. deposited ultra-small (< 2 nm) Pt and Au nanoparticles by this method [11]. The size and coverage of deposited metal nanoparticles were controlled by the discharge parameters. However, the transport and size modification of micro-particles during MCVAs deposition process are still open challenges for the preparation of hard coatings and other functional nanoparticles until now.

Several approaches have been adopted to control the amount of micro-particles, such as a modified magnetic field, filtering, optimized working pressure and substrate bias [6]. The formation of micro-particles is directly relevant to the emission of micro-droplets during the movement of arc spots. With the assistance of magnetic field, the location and motion of the arc spots can be confined to desired surfaces, which affects the emission of micro-droplets and the quality of subsequent deposited coatings [12,13]. Therefore, it is important to investigate the dependence of cathodic arc spot motion behaviors on magnetic field [14]. Many works have been conducted, such as the magnetic field configuration [15], the confining of arc plasma [16,17] and continuous arc spot motion [13,18], etc... Particularly, the anomalous retrograde motion of arc spots once puzzled the researchers [19,20], then was clarified by K.C. Lee et al. [21] I.I. Beilis systematically studied the cathodic vacuum arc spot motion [22,23], splitting [24] and grouping phenomenon [25,26] in oblique magnetic field. As comprehensive researches on the parameters of arc spot motion of continuous arc have been carried out, advanced applications of MCVAs are able to be realized. For example, T. Zhuang et al. built a small arc plasma source with cathode spot moving circularly by magnetic field confinement, which leaded to the possibility of creating a circularly moving plasma plume [27]. However, the relationship between arc spot movement and micro-particle size is unclear. The possibility of controlling the micro-particle size still remain debatable.

* Corresponding author. Key Laboratory of Marine Materials and Related Technologies, Zhejiang Key Laboratory of Marine Materials and Protective Technologies, Ningbo Institute of Materials Technology and Engineering, Chinese Academy of Sciences, Ningbo, 315201, China.

E-mail address: aywang@nimte.ac.cn (A. Wang).

[1] X. Zuo and R. Chen contributed to this work equally.

https://doi.org/10.1016/j.vacuum.2019.03.048

Received 2 January 2019; Received in revised form 7 March 2019; Accepted 23 March 2019

Available online 26 March 2019

0042-207X/

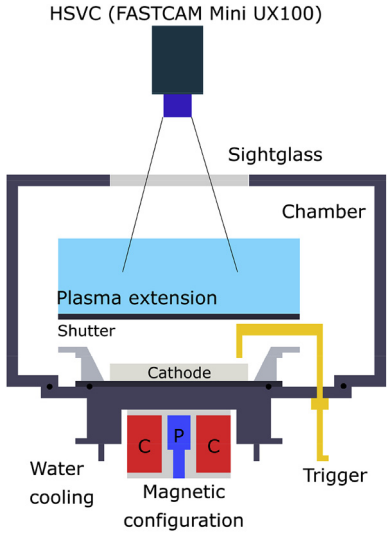

Fig. 1. The schematic graph of the vacuum cathodic arc equipment and HSVC. '*P*' and '*C*' presents the permanent magnets and electromagnet coil winding, respectively.

Therefore, the dynamics of cathodic arc spot motion are the key subjects of researches on the preparation of hard coatings and nano-materials. Particularly, the regulation of micro-particles distribution through the modification of arc spot motion become more and more attractive. The objective of this work is to further determine the motion mode of the cathodic arc spots, and subsequent spot position and size distribution at different arc current and magnetic field conditions. Finally, the size modification of metal micro-particles can be realized.

2. Experimental setup

2.1. Cathodic vacuum arc source and high speed imaging

Fig. 1 is a schematic graph of the cathodic vacuum arc source. A circular planar Ti target (99.9%) is clamped to a copper backing plate which is cooled by water. The target size is Φ12.8 cm × 1.5 cm. Cylindrical NdFeB magnets (tagged as '*P*') are used to generate a static magnetic field. An electromagnetic coil winding (tagged as '*C*') can produce variable opposite magnetic field by changing the coil current. Magnetic field in the Ti target surface was measured by a Gauss meter (HT201 Gaussmeter, Hengtong magnetoelectricity CO., LTD.). The chamber was pumped to a base pressure of 1.3×10^{-3} Pa. The working pressure was maintained at 5.3 Pa with 100 sccm Ar gas (99.99%). The cathode was supplied through a DC power unit (IDU-200N, EN Technologies Inc.) and ignited by a pneumatic tungsten trigger. Cathodic arc spots were monitored by a high speed video camera (HSVC, FASTCAM Mini UX100) with 1280 × 1024 pixels at 2400 frames/s. The HSVC viewing axis intersected the center of the cathode through a glass window. The arc was triggered and burnt for 10 min to remove surface contamination, and then the shutter was removed. After that, the HSVC started recording and continued for 1.0 s. Then the glass was substituted by a new clean one.

2.2. Image processing

The HSVC images were extracted frame by frame by using the Photron FASTCAM Viewer (PFV 2.11E) software. Each frame was binarized, the edge of each spot was detected and circle fitted to obtain the center coordinates and radius of each spot. Therefore, the movement of arc spot with time was clarified. Fig. 2 demonstrates a part of spot motion trajectory when arc current is 60 A. The motion trajectory of luminous group spots (GSs) isn't smooth, additional stochastic motion is observed. Because the cathode doesn't have a mirror surface, the motion of GSs is affected by the surface texture of the cathode [28,29]

Each HSVC recording had 2400 frames. The first 1800 frames were selected, the spots were analyzed and integrated in a single figure. The kernel density estimation (KDE) method was applied to obtain the distribution of spots size and position under various arc current and coil current conditions [30]. The kernel density estimator and bandwidth was selected as 'Gaussian' and 'Silverman', respectively. Spot velocity and deflection angle were evaluated by the distance between two spot centers on sequential frames and time between recording those frames.

2.3. Measurement of the average size of Ti micro-particles

Metal Ti coatings were deposited on Si substrates (10 × 10 mm^2) to measure the size of micro-particles. The substrate-target distance was 12 cm and deposition time was 40 min. No additional heating and substrate bias were applied. The surface and cross-sectional morphology of the Ti coatings were characterized by scanning electron microscope (SEM, FEI Quanta FEG 250). The size of micro-particles embedded in the coating was statistically measured from cross-sectional SEM images through Nano Measurer 1.2 software (*Developed by Department of Chemistry, Fudan University*). Thus the average size of micro-particles under different arc current and coil current conditions could be calculated.

3. Results and discussions

3.1. Magnetic field distribution of the cathodic arc source

The distributions of magnetic field components (B_r, B_z) in the circular planar cathode surface were shown in Fig. 3. When the coil current raised from 0.0 A to 0.5 A, both of the radial and normal component of the magnetic field were significantly weakened. As the coil current increased to 1.5 A, the combination of permanent magnets and the coil winding resulted in a slight magnetic field which only distributed in the central region of the cathode surface. When the coil current was higher than 2.5 A, the directions of both radial and normal magnetic fields reversed. Except the observed changes in the magnitude and direction of the magnetic field components, the radial position corresponding to the maximum of radial magnetic field moved inwards the center of the cathode surface when the coil current was increased from 0.0 A to 1.5 A. However, further increasing the coil current leaded to an outwards movement of the maximum radial magnetic field position.

3.2. Dynamics of luminous group spots motion with the variation of arc currents

First the influence of the arc current on the motion of the GSs is investigated without setting coil current (0 A). The size of GSs in HSVC recordings is 0.4–1.4 mm in diameter. Fig. 4 shows the position and size distribution of the GSs. GSs overlapped with each other evidently as time went on. So the statistic bivariate KDE method was applied to find the GSs position probability distributions (GSPPDs). The corresponding GSPPDs were figured out in Fig. 4(a')–(e'). Apparently, the GSs distributed non-uniformly in the cathode surface. Most of the GSs distributed at an annulus region between the cathode center and cathode boundary. Overall, GSPPDs didn't show distinct differences when the arc current decreased from 100 A to 60 A. However, the GSs size probability distributions (GSSPDs) were greatly affected by the arc current. The GSSPDs were obtained through histograms and KDE methods in Fig. 4(a")–(e"). With the reduction of arc current, the size of GSs decreased. Furthermore, when the arc current was reduced to 80 A, the GSSPDs changed from bi-modal to unimodal distribution. There were two groups of GSs with different sizes when the arc current was

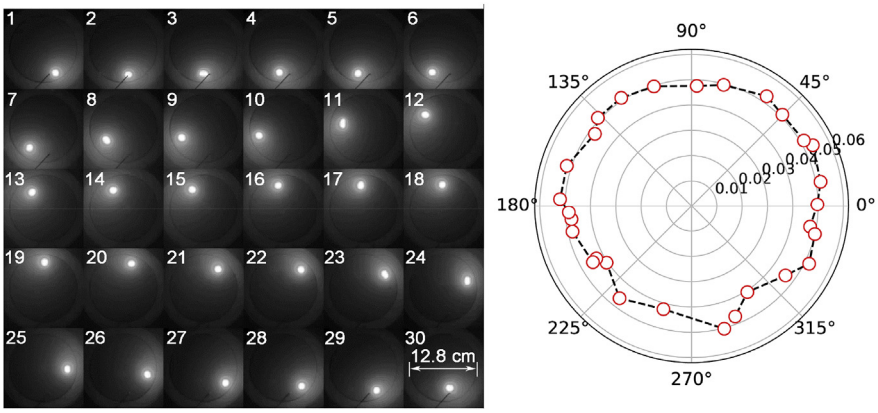

Fig. 2. Images of partial cathodic spots and its trajectory with 60 A arc current.

greater than or equal to 90 A. This phenomenon could be attributed to the splitting of the cathode spot at high current conditions [31]

The size of an arc spot is a function of the heat on each spot location [32]. It is known that spots ignite and decay on a sub-microsecond time scale [20]. Therefore, each GSs should contain several hundred even thousands of spots. The heat (Q_{arc}) produced by arc current (I_{arc}) in spot residence time (t_r) can be expressed according to Joule's first law:

$$Q_{arc} \propto I_{arc}^2 \cdot t_r \tag{1}$$

The background local heat density (q_{loc}) is the residual heat over the cathode surface:

$$q_{loc.} = \frac{Q_T}{S_{cov.}} - \frac{Q_{cool}}{A} \tag{2}$$

$$q_{loc.} \propto \frac{I_{arc}^2 \cdot T}{S_{cov.}} - \frac{Q_{cool}}{A} \tag{3}$$

Where, $q_{loc} \geq 0$, Q_T is the arc heating energy, and Q_{cool} is thermal energy carried away during working time (T) by water coolant, thermal radiation process and so on. $S_{cov.}$ is the coverage area of GSs positions on the cathode. A is the area of cathode surface. Therefore, the total heat density ($q_{tot.}$) on an arc spot site can be written in the following formula:

$$q_{tot.} = \frac{Q_{arc}}{\varphi} + q_{loc.} \tag{4}$$

$$q_{tot.} \propto I_{arc}^2 \cdot t_r \left(\frac{1}{\varphi} + \frac{T}{t_r} \cdot \frac{1}{S_{cov.}} \right) - \frac{Q_{cool}}{A} \geq 0 \tag{5}$$

$$\frac{1}{\varphi} > \frac{1}{t_r} \left(\frac{Q_{cool}}{I_{arc}^2 \cdot A} - \frac{T}{S_{cov.}} \right) \tag{6}$$

where, φ is the spot size. It can be found that the spot size was affected by the arc current, residence time, and coverage area. As shown in Fig. 4(a')-(e') the coverage area of GSs changes little under different arc current conditions. The residence time should be determined by the velocity of arc spots. In polar coordinate system, this velocity could be decomposed into rotation velocity ($v_{rot.}$) and scan velocity ($v_{sca.}$). The relationship between these velocities and arc current has be proposed by I.I. Beilis [23],

$$v_{rot.} \propto (I_{arc} \cdot B_r)^{1/2} \tag{7}$$

$$v_{sca.} \propto (I_{arc} \cdot B_r)^{1/4} \cdot B_z^{1/2} \tag{8}$$

where, B_r and B_z (as shown in Fig. 5(b)) is the magnetic field component in r and z direction, respectively. Therefore, the spot size still has a positive correlation with arc current.

Furthermore, the motion of GSs on the cathode surface was analyzed based on the HSVC recordings. The distance (d) between two adjacent GSs, moving velocity (v) and angle (α) were evaluated by the determined coordinates (x,y) and (x',y') of GSs center on sequential

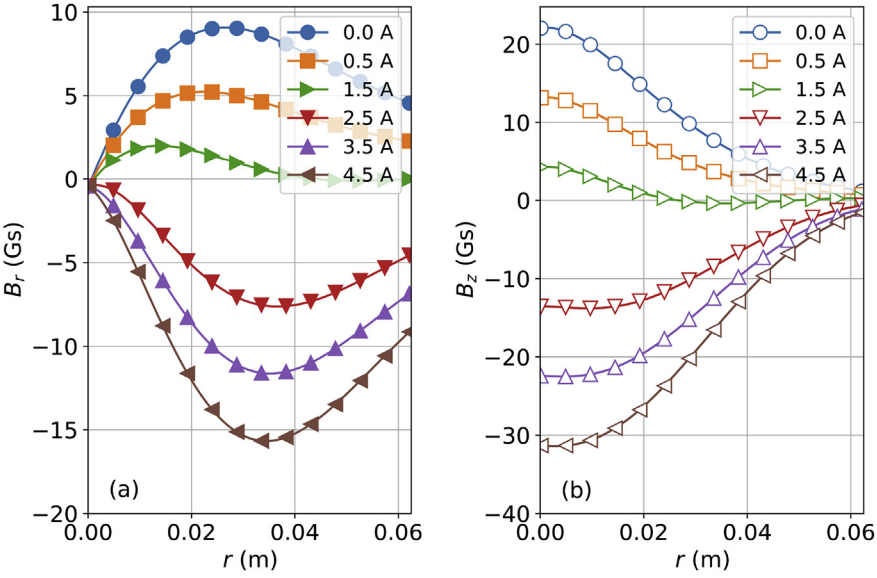

Fig. 3. The radial distribution of (a) radial and (b) normal components of magnetic field (B_r and B_z) in the cathode surface.

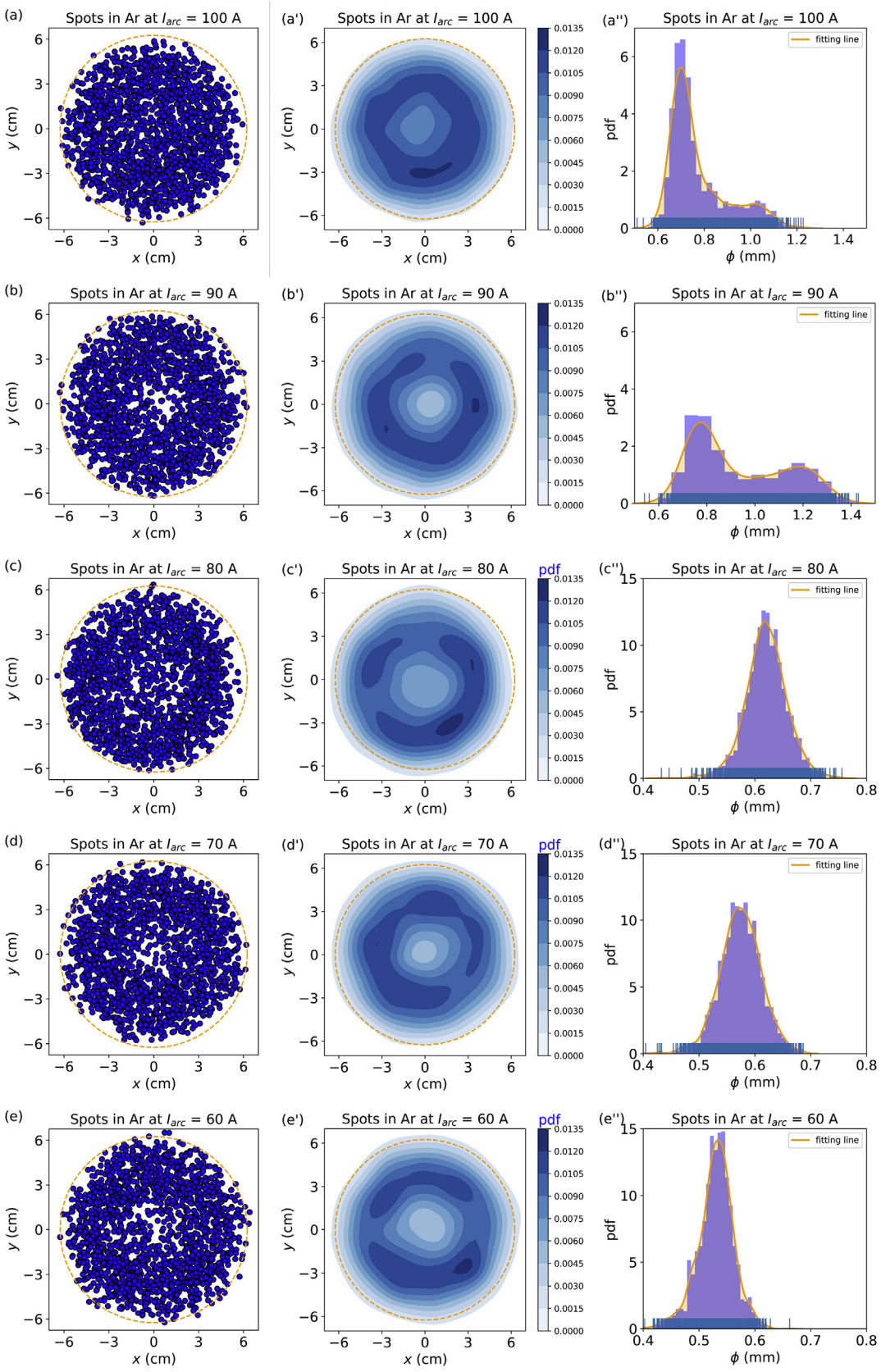

Fig. 4. The GSs in the cathode surface (a–e), and their corresponding GSPPDs (a'-e'), and GSSPDs (a"-e") when the arc current was changed from 100 A to 60 A. Blue circles represent the GSs. The orange dash line indicates the cathode boundary. ϕ is the size of the GSs. (For interpretation of the references to colour in this figure legend, the reader is referred to the Web version of this article.)

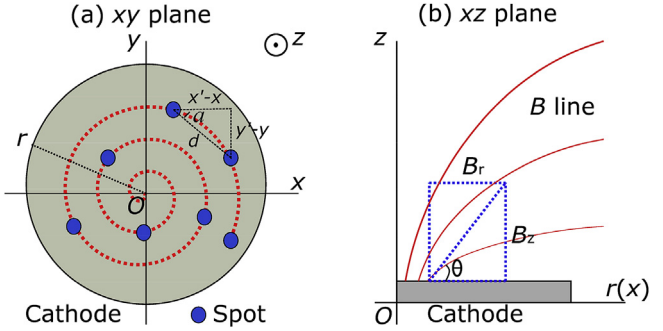

Fig. 5. Top and cross view of schematic graphs showing (a) the motion of GSs and (b) magnetic field lines, respectively.

frames, defined in Fig. 5(a). Parameters, like d, v, and α, can be calculated by the following formulas:

$$d = \sqrt{(x' - x)^2 + (y' - y)^2} \tag{9}$$

$$v = \frac{d}{t_{\text{lag}}} \tag{10}$$

$$\tan(\alpha) = \frac{y' - y}{x' - x} \tag{11}$$

where, $t_{\text{lag}} \approx 0.42$ ms is the time between the two adjacent GSs.

Fig. 6(a)-(e) shows the temporal evolutions of GSs velocity at different arc current values. As arc current decreased from 100 A to 60 A, the velocity of GSs reduced from ~5.0 m/s to ~2.5 m/s. The velocity also presented stochastic fluctuations. This could be explained that besides being affected by arc current and magnetic field, the GSs motion was also affected by the surface texture of the cathode. The temporal evolutions of the moving angle at different arc current values are also plotted in Fig. 6(a')-(e'). It illustrates clearly that the moving angle changes periodically with running time. The time between two positive peaks was a period of GSs' one lap motion. It decreased and increased alternately with time, which indicated that the GSs took spiral motion on the cathode. The GSs took similar motion with the arc current at 100 A, 90 A and 80 A. Further lowering down the arc current, the period of moving angle got longer, and the irregular jump of GSs became more apparent.

The average scan velocity ($v_{\text{sca.}}$) and rotation velocity ($v_{\text{rot.}}$) between any two adjacent GSs are calculated by the following equations though their center coordinates:

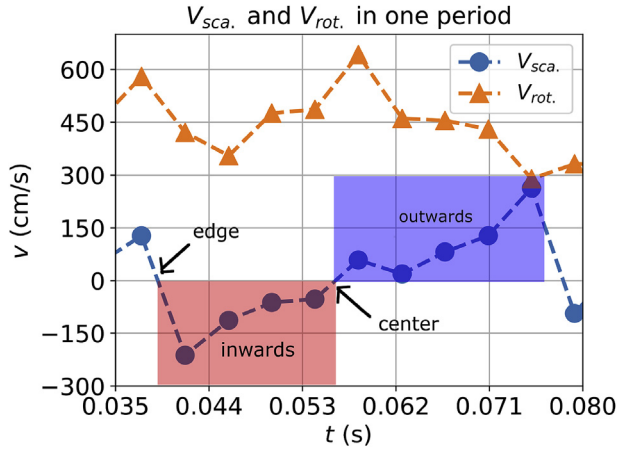

Fig. 7. The variation of rotation and scan velocities ($v_{\text{rot.}}$ & $v_{\text{sca.}}$) during a lap motion.

$$v_{\text{sca.}} = \frac{\sqrt{x'^2 + y'^2} - \sqrt{x^2 + y^2}}{t_{\text{lag}}} \tag{12}$$

$$v_{\text{rot.}} = \frac{2\sqrt{(x^2 + y^2)(x'^2 + y'^2)} - 2(xx' + yy')}{t_{\text{lag}}} \tag{13}$$

Take the GSs motion with arc current at 100 A for example, the variations of the two velocities with time in a lap motion are shown in Fig. 7. The negative sign of the scan velocity indicates the GSs move inwards to the center of the cathode. As the velocity changes to be positive, GSs start moving outwards to the boundary of the cathode. The scan velocity of GSs decreases when moving inwards from the periphery region of the cathode, then has a slight increase when moving close to the center region of the cathode. The rotation velocity also increases at the periphery and center region of the cathode. When the velocities are slow, the position probability of GSs is high. Therefore, the GSs position probability distributions presented in Fig. 4(a')-(e') are halo-like.

3.3. Dynamics of the luminous group spots motion with the variation of coil currents

Furthermore the influence of magnetic field on the GSs motion was investigated with arc current at 60 A through changing the coil current. The direction of magnetic field generated by the coil winding is

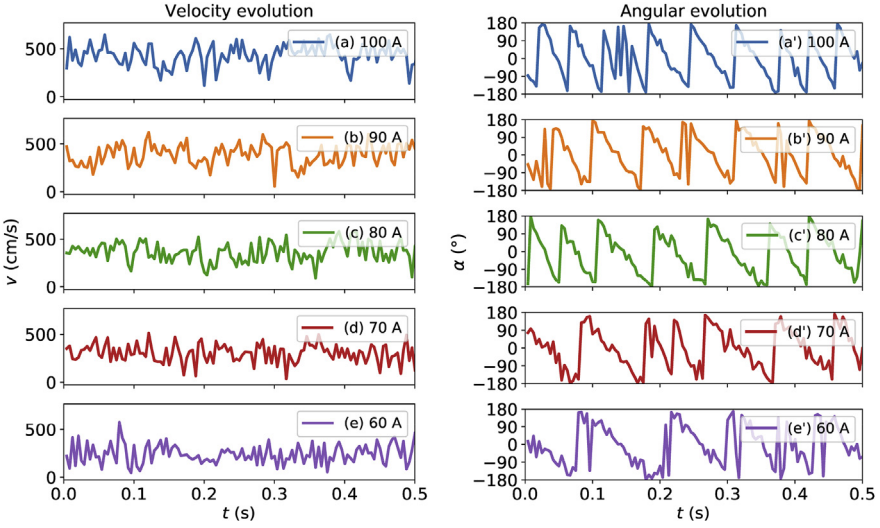

Fig. 6. The velocity (v) and angular (α) evolutions of arc spots on Ti cathode with the variation of arc current from 100 A to 60 A.

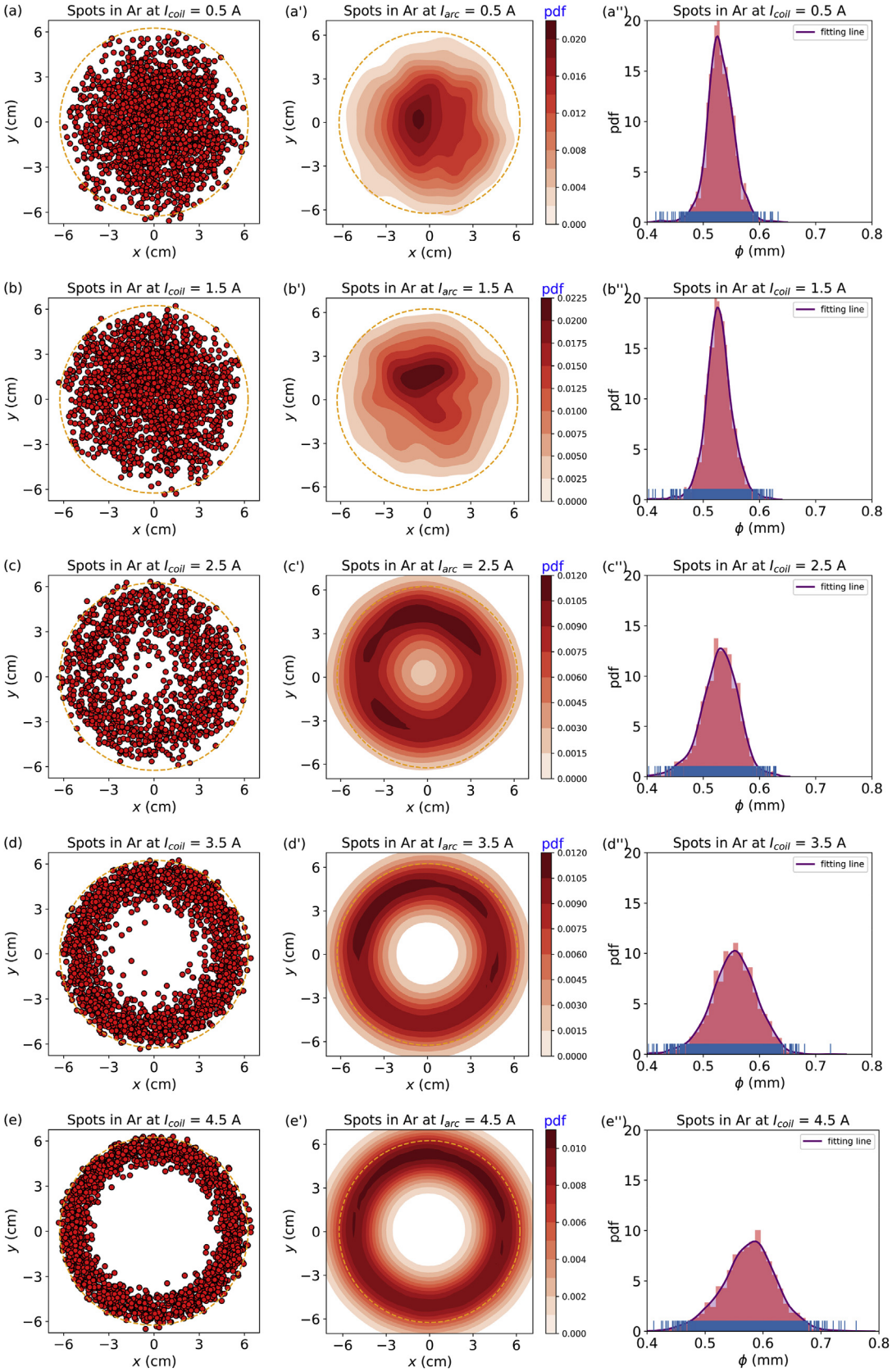

Fig. 8. The position distribution (a–e), position probability distribution (a'-e'), and size distribution of GSs (a''-e') with the variation of coil current from 0.5 A to 4.5 A. Red circles represent the GSs. The orange dash line indicates the cathode boundary. ϕ is the size of the GSs. (For interpretation of the references to colour in this figure legend, the reader is referred to the Web version of this article.)

opposite with the direction of the permanent magnetic field. Therefore, the resultant magnetic field could vary in magnitude with a wide range. Fig. 8 presents the variation of GSs position and size distributions with coil currents. With the increase of coil current, GSs position distribution on the cathode changed dramatically. When the coil current was 0.5 A and 1.5 A, the position distribution of GSs tended to concentrate on the central region of the cathode surface (Fig. 8(a')-(b')). As the coil current increased to 2.5 A, GSs moved outwards from the center, the GSs position probability distribution turned into a similar form in Fig. 4. Further increasing the coil current to 3.5 A and 4.5 A, GSs just moved on the periphery of the cathode (Fig. 7(d')-(e')). However, the GSPPDs in Fig. 7(d')-(e') deviated apparently from the measured GSs position distributions in Fig. 7(d)-(e). This is because only 'Gaussian' estimator could be used in bivariate KDE method. However, the GSPPDs in Fig. 7(d')-(e') were still provided for reference. With the variation of coil current, arc voltage kept constant at 17 ± 1 V all the time. Therefore, as the coverage of GSs position on the cathode became smaller, the residual local energy density on covered area grew higher. Thus, an improvement of GSs size was observed when the coil current increased from 1.5 A to 4.5 A.

The dynamical parameters on GSs motion under different coil current conditions are presented in Fig. 9. The velocity of GSs motion reached a minimum at 1.5 A. Compared with the GSs velocity at 60 A without coil current condition in Fig. 6(a), it decreased to ~2.3 m/s. Further increasing the coil current to 4.5 A, the velocity was improved to ~6.3 m/s. The GSs motion behaviors can also be inferred out from the variation of moving angle with running time in Fig. 9(b). When the coil current was 0.5 A and 1.5 A, the periodic variation of moving angle vanished, the movement of GSs was dominated by stochastic motion. However, as the coil current increased to 2.5 A, the variation of moving angle presented periodic feature again which indicated spiral motion of GSs again. When the coil current increased to 4.5 A, the period of moving angle kept nearly constant. The GSs changed into circular motion at the periphery of the cathode. The change of GSs motion behaviors had direct relationship with the variation of magnetic field. Assuming that the influence of self-induced magnetic field by arc current could be neglected, magnetic field distributions under various coil current on the Ti cathode were shown in Fig. 3.

I.I. Beilis has developed a model of vacuum cathodic arc spot motion in magnetic field [23]. According to the model, rotation velocity and scan velocity can be written in the following equations:

$$v_{\mathrm{rot.}} = \left(\frac{I_{\mathrm{arc}} B_{\mathrm{r}}}{\pi m n_{\mathrm{h}} r_{\mathrm{ef}}}\right)^{1/2} \tag{14}$$

$$v_{\mathrm{sca.}} = \left(\frac{2\mathrm{e} v_{\mathrm{rot.}} B_{\mathrm{z}} r_{\mathrm{ef}} n_{\mathrm{sp}}}{m n_{\mathrm{h}}}\right)^{1/2} \tag{15}$$

where, r_{ef} is the distance in the x direction from the center of the "old" cathode spot to the location, m is the atom mass, n_{h} is the heavy particle density, e is elementary charge, and n_{sp} is a positive space charge formed in the plasma in pre-sheath. Thus, the expression of the ratio (γ_{d}) between scan velocity and rotation velocity can be written as follows:

$$\frac{v_{\mathrm{sca.}}}{v_{\mathrm{rot.}}} = C \cdot I_{\mathrm{arc}}^{-1/4} \left(\frac{B_{\mathrm{z}}^2}{B_{\mathrm{r}}}\right)^{1/4} \tag{16}$$

$$C = (2 e n_{\mathrm{sp}})^{1/2} \left(\frac{\pi r_{\mathrm{ef}}^3}{m n_{\mathrm{h}}}\right)^{1/4} \tag{17}$$

where, C is a parameter which doesn't depend on arc current and magnetic field. The oblique angle of magnetic field (B) to the cathode surface was signed as θ in Fig. 5(b). Since $B_{\mathrm{r}} = B\cos\theta$, $B_{\mathrm{z}} = B\sin\theta$, γ_{d} can be also expressed in the following form:

$$\gamma_{\mathrm{d}} = C \cdot I_{\mathrm{arc}}^{-1/4} \left(B\left(\frac{1}{\cos\theta} - \cos\theta\right)\right)^{1/4} \tag{18}$$

The variation of γ_{d} along r direction under different arc current and coil current conditions are presented in Fig. 10. Overall, γ_{d} reduces along the r direction, which is mainly determined by the $B(r)$ distribution. It reflects the offset of GSs motion in the tangent direction. Thus Fig. 10(a)–(b) indicates the offset of the GSs velocity in the direction of rotation velocity. The higher this value is, the larger the deviation angle will be. As a consequence, the number of GSs captured by the HSVC would increase in r direction. However, this trend is inconsistent with the measurement results in Fig. 4(a'-e'), because I.I, Beilis et al. assumes that the electric field distributes uniformly. The non-uniform electric field at the edge of the cathode would depress the GSs motion toward the periphery of the cathode. With the decrease of arc current to 60 A, γ_{d} was slightly reduced. The difference in GSs position probability distributions caused by such small changes wasn't visibly observed in Fig. 4. Meanwhile, γ_{d} changes obviously with the coil current. As the coil current increased to 1.5 A, γ_{d} lowered down apparently which indicated the movement of GSs to the central region of the cathode. When the coil current was higher than 1.5 A, γ_{d} tended to increase. γ_{d} at 2.5 A regained similar distribution with that of 0 A,

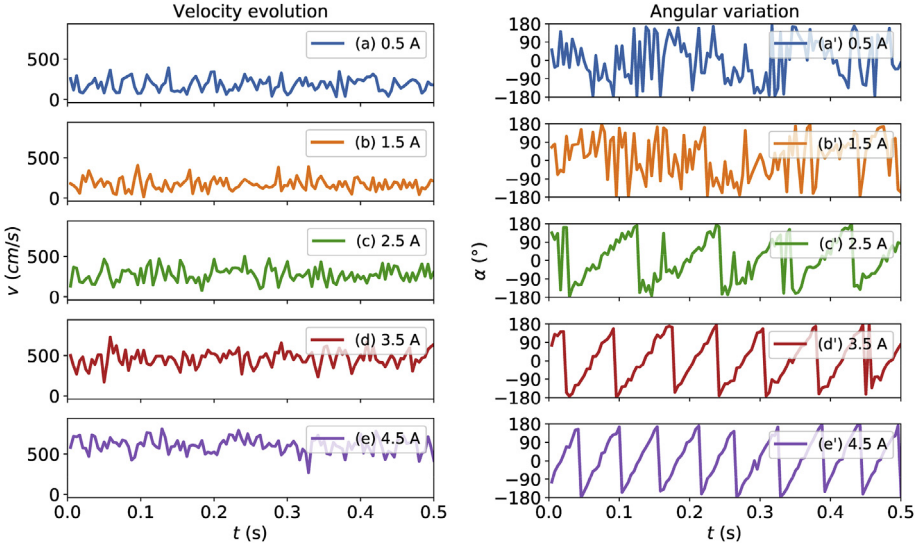

Fig. 9. The velocity and angular evolutions of GSs on Ti cathode with the variation of coil currents from 0.5 A to 4.5 A.

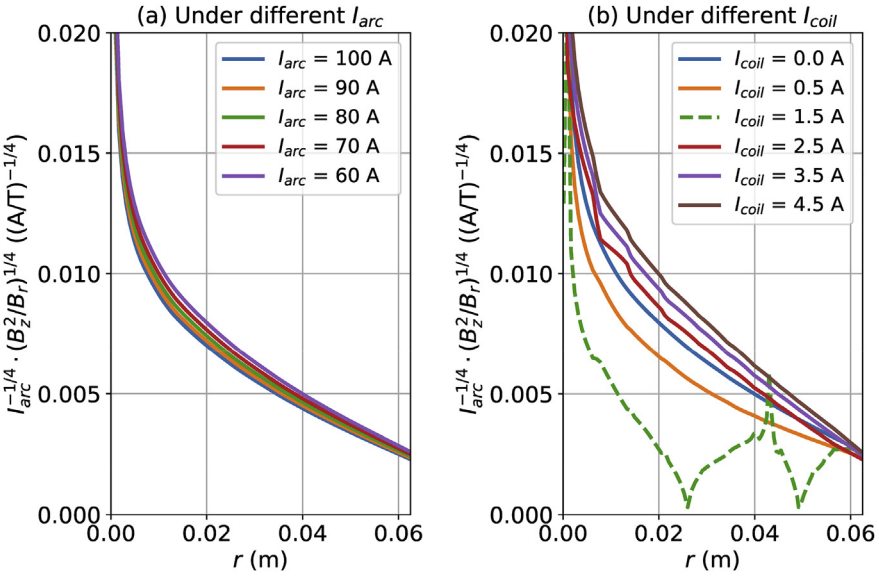

Fig. 10. The radial distribution of γ_d/C under different arc current and coil current conditions.

thus similar GSSPDs were obtained. As γ_d expanded outward continuously at 3.5 A and 4.5 A, GSs finally moved in circles at the periphery region of the cathode surface.

3.4. Size modification of Ti micro-particles

Fig. 11(a) shows the average size (Φ_a) of Ti micro-particles under various arc currents. With the decrease of arc current from 100 A to 60 A, the micro-particle size reduced from ~0.88 μm to ~0.56 μm. The generation of micro-particles in arc deposition derived from the micro-droplets emitted from arc spots. The size of micro-droplets was affected by the thermal energy accumulated on the arc spots during their residence time. Therefore, according to Equ. (3)–(4), the size of the arc spots was expected to reduce with the decline of arc current. As a result, the average size of emitted micro-droplets became smaller. The micro-droplets cooled down after leaving the cathode, and the incidence of them on the substrate generated micro-particles. Therefore, the change of micro-particles size with arc current showed a consistent relationship with the variation of GSs size distribution.

The variation of micro-particle size with the increase of coil current from 0.5 A to 4.5 A is demonstrated in Fig. 11(b). When the coil current increased to 2.5 A, the average size of micro-particles decreased to ~0.39 μm. However, further rising coil current to 4.5 A, the size increased to ~0.70 μm. This variation tendency of micro-particle size with coil current didn't correspond to that of GSs size presented in Fig. 8(a")-(e"). In Fig. 8(a')-(e') with the increase of the coil current, the GSs position probability distributions changed from center-concentration to dispersion, and then to periphery-concentration. As the GSs position probability distributions on the Ti cathode changed significantly with the increase of coil current, the incident angle of micro-droplets on the substrate would be different. A change in incident angle would result in a different size distribution of micro-particles from that of GSs [7,33]. At 2.5 mTorr, most of the GSs distributed in an annulus region with a radius ~3 cm, the emission angle with respect to the

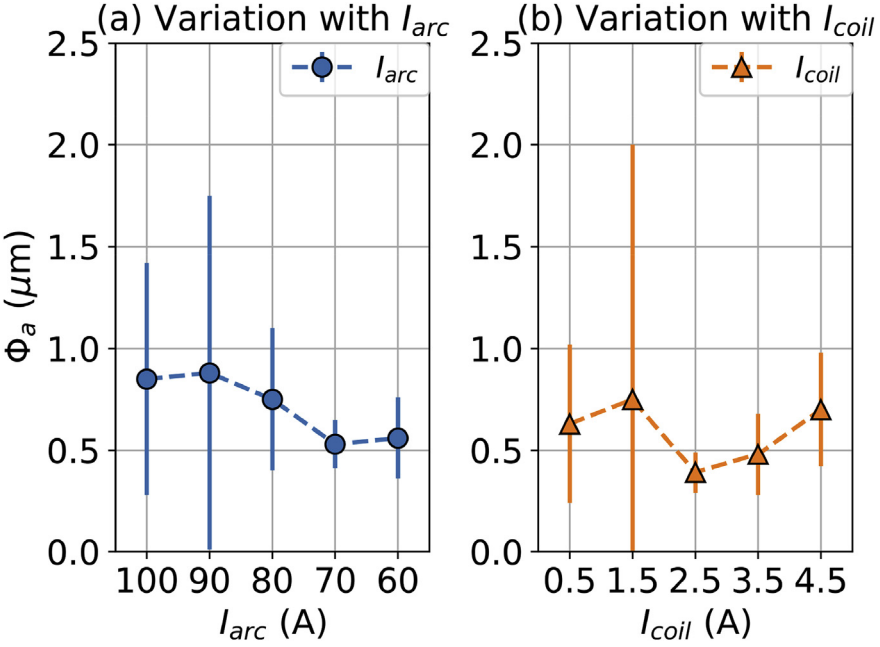

Fig. 11. Size distribution of micro-particles with the variation of arc current (a) and coil current (b). Φ_a is the average size of micro-particles.

plane of the cathode was ~75.9°. As the coil current increased to 4.5 A, the radius increased to ~5 cm, the emission angle decreased to ~66.9°. It is known that the micro-particles are emitted preferentially an angle of 60° to the plane of the Ti target for TiN coatings. At larger angles preferentially smaller macroparticles are observed [34].

4. Conclusions

The configuration combining permanent magnets with electromagnetic coil winding was applied to realize the control on GSs position and size distributions in MCVA discharge. The GSs motion behaviors on Ti cathode and the modification of micro-particles had been investigated. GSs position distribution was mainly determined by magnetic field distribution rather than the arc current. But the GSs size could be adjusted by arc current. When the arc current decreased from 100 A to 60 A, the GSs size decreased to around 0.55 mm. Additionally, GSs size probability distribution changed from bimodal distribution to unimodal distribution with arc current at 90 A. GSs movement at these conditions was dominated by spiral motion. Different GSs position probability distribution and GSs motion behaviors were achieved by regulating the magnetic field on the cathode. As the magnetic field was weakened significantly with the coil current at 0.5 A and 1.5 A, GSs distributed at the center region of the cathode, the GSs movement was stochastic motion dominated. Further increasing the coil current higher than 3.5 A, GSs changed to distribute at the periphery region of the cathode and took circular motions. The variation tendencies of GSs size and micro-particles size were consistent with each other until the coil current higher than 2.5 A.

Acknowledgements

This work was supported by the National Natural Science Foundation of China (11705258, 51522106), Ningbo Science and Technology Inovation Project (2018B10014), as well as the Special Research and Development Project of Jiangxi Province (2018-YZD2-15). The authors would like to thank Dr. Longyang Li and Prof. Zhixiang Zeng for his assistance with the HSVC measurements.

References

[1] A. Anders, Metal plasmas for the fabrication of nanostructures, J. Phys. D Appl. Phys. 8 (2007) 2272–2284.
[2] P.J. Martin, A. Bendavid, Review of the filtered vacuum arc process and materials deposition, Thin Solid Films 1–2 (2001) 1–15.
[3] M. Medhisuwakul, N. Pasaja, S. Sansongsiri, J. Kuhakan, S. Intarasiri, L.D. Yu, Development and application of cathodic vacuum arc plasma for nanostructured and nanocomposite film deposition, Surf. Coating. Technol. (2013) 36–41.
[4] I. Zhirkov, A. Petruhins, L.A. Naslund, S. Kolozsvari, P. Polcik, J. Rosen, Vacuum arc plasma generation and thin film deposition from a TiB2 cathode, Appl. Phys. Lett. 18 (2015) 184103.
[5] A. Anders, Metal plasma immersion ion implantation and deposition: a review, Surf. Coating. Technol. 2–3 (1997) 158–167.
[6] R.L. Boxman, V.N. Zhitomirsky, Vacuum arc deposition devices, Rev. Sci. Instrum. 2 (2006) 021101.
[7] H.T.C. Kaufmann, M.D. Cunha, M.S. Benilov, W. Hartmann, N. Wenzel, Detailed numerical simulation of cathode spots in vacuum arcs: interplay of different mechanisms and ejection of droplets, J. Appl. Phys. 16 (2017) 163303.
[8] C.L. Chang, C.T. Ho, P.H. Chen, W.C. Chen, D.Y. Wang, W.Y. Wu, Synergetic effect for improved deposition of titanium nitride films, Surf. Coating. Technol. (2018) 1098–1104.
[9] I. Zhirkov, A. Petruhins, J. Rosen, Effect of cathode composition and nitrogen pressure on macroparticle generation and type of arc discharge in a DC arc source with Ti-Al compound cathodes, Surf. Coating. Technol. (2015) 20–26.
[10] Y. Xu, J.Y. Yang, M. Demura, T. Hara, T. Hirano, Y. Matsushita, M. Tanaka, Y. Katsuya, Fabrication of Ni-Al nanoparticles via vacuum arc plasma evaporation and their catalytic properties for CO oxidation, Appl Catal a-Gen (2014) 165–174.
[11] S.H. Kim, Y.E. Jeong, H. Ha, J.Y. Byun, Y.D. Kim, Ultra-small platinum and gold nanoparticles by arc plasma deposition, Appl. Surf. Sci. (2014) 52–58.
[12] S.H. Wang, Z. Lin, H. Qiao, D.C. Ba, L.D. Zhu, Influence of a scanning radial magnetic field on macroparticle reduction of arc ion-plated films, Coatings 2 (2018) 49.
[13] X. Song, Q. Wang, Z. Lin, P.H. Zhang, S.H. Wang, Control of vacuum arc source cathode spots contraction motion by changing electromagnetic field, Plasma Sci. Technol. 2 (2018) 025402.
[14] Z.L. Tang, K. Yang, H.X. Liu, Y.C. Zhang, H. Li, X.D. Zhu, Dynamics of cathode spots in low-pressure arc plasma removing oxide layer on steel surfaces, Phys. Plasmas 3 (2016) 033501.
[15] A.P. Ehiasarian, P.E. Hovsepian, R. New, J. Valter, Influence of steering magnetic field on the time-resolved plasma chemistry in cathodic arc discharges, J. Phys. D Appl. Phys. 15 (2004) 2101–2106.
[16] J. Rosen, A. Anders, J.M. Schneider, Plasma chemistry fluctuations in a reactive arc plasma in the presence of magnetic fields, Appl. Phys. Lett. 22 (2002) 4109–4111.
[17] R. Sangines, A.M. Israel, I.S. Falconer, D.R. McKenzie, M.M.M. Bilek, Production of highly ionized species in high-current pulsed cathodic arcs, Appl. Phys. Lett. 22 (2010) 221501.
[18] A.L. Garner, Cathode spot motion in an oblique magnetic field, Appl. Phys. Lett. 1 (2008) 011505.
[19] B. Juttner, Cathode spots of electric arcs, J. Phys. D Appl. Phys. 17 (2001) R103–R123.
[20] B. Juttner, I. Kleberg, The retrograde motion of arc cathode spots in vacuum, J. Phys. D Appl. Phys. 16 (2000) 2025–2036.
[21] K.C. Lee, Gyrocenter shift of low-temperature plasmas and the retrograde motion of cathode spots in arc discharges, Phys. Rev. Lett. 6 (2007) 065003.
[22] I.I. Beilis, B. Sagi, V. Zhitomirsky, R.L. Boxman, Cathode spot motion in a vacuum arc with a long roof-shaped cathode under magnetic field, J. Appl. Phys. 23 (2015) 233303.
[23] I.I. Beilis, Vacuum arc cathode spot motion in oblique magnetic fields: an interpretation of the Robson experiment, Phys. Plasmas 9 (2016) 093501.
[24] I.I. Beilis, Mechanism of cathode spot splitting in vacuum arcs in an oblique magnetic field, Phys. Plasmas 10 (2015) 103510.
[25] I.I. Beilis, Vacuum arc cathode spot grouping and motion in magnetic fields, IEEE Trans. Plasma Sci. 6 (2002) 2124–2132.
[26] I.I. Beilis, Mechanism for cathode spot grouping in vacuum arcs, Appl. Phys. Lett. 21 (2002) 3936–3938.
[27] T. Zhuang, A. Shashurin, M. Keidar, I.I. Beilis, Circular periodic motion of plasma produced by a small-scale vacuum arc, Plasma Sources Sci. Technol. 1 (2011) 015009.
[28] J.Q. Zhu, B. Syed, P. Polcik, G. Hakansson, M. Johansson-Joesaar, M. Ahlgren, M. Oden, Effects of the cathode grain size and substrate fixture movement on the evolution of arc evaporated Cr-cathodes and Cr-N coating synthesis, J. Vac. Sci. Technol. A 2 (2014) 021515.
[29] Y.P. Wang, C.Y. Zhang, H. Zhang, B.J. Ding, K. Lu, Effect of the microstructure of electrode materials on arc cathode spot dynamics, J. Phys. D Appl. Phys. 21 (2003) 2649–2654.
[30] F. Pedregosa, G. Varoquaux, A. Gramfort, V. Michel, B. Thirion, O. Grisel, M. Blondel, P. Prettenhofer, R. Weiss, V. Dubourg, J. Vanderplas, A. Passos, D. Cournapeau, M. Brucher, M. Perrot, E. Duchesnay, Scikit-learn: machine learning in Python, J. Mach. Learn. Res. (2011) 2825–2830.
[31] B.E. Djakov, R. Holmes, Cathode spot division in vacuum arcs with solid metal cathodes, J. Phys. D Appl. Phys. 4 (1971) 504–509.
[32] A.G. Parfyonov, Concerning the types of cathode spots, IEEE Trans. Plasma Sci. 5 (1985) 277–280.
[33] P.D. Swift, Macroparticles in films deposited by steered cathodic arc, J. Phys. D Appl. Phys. 7 (1996) 2025–2031.
[34] A.W. Baouchi, A.J. Perry, A study of the macroparticle distribution in cathodic-arc-evaporated TiN films, Surf. Coating. Technol. 49 (1991) 253–257.